

CaTe: a new topological node-line and Dirac semimetal

Yongping Du¹, Feng Tang¹, Di Wang¹, Li Sheng^{1,2}, Er-jun Kan³,
Chun-Gang Duan⁴, Sergey Y. Savrasov⁵ and Xiangang Wan^{1,2*}

¹National Laboratory of Solid State Microstructures and Department of Physics, Nanjing University, Nanjing 210093, China

²Collaborative Innovation Center of Advanced Microstructures, Nanjing University, Nanjing 210093, China

³Key Laboratory of Soft Chemistry and Functional Materials (Ministry of Education), and Department of Applied Physics, Nanjing University of Science and Technology, Nanjing, Jiangsu 210094, P. R. China.

⁴Key Laboratory of Polar Materials and Devices, Ministry of Education, East China Normal University, Shanghai 200062, China

⁵Department of Physics, University of California, Davis, One Shields Avenue, Davis, California 95616, USA

(Dated: August 20, 2018)

Topological semimetals recently stimulate intense research activities. Combining first-principles calculations and effective model analysis, we predict that CaTe is topological node-line semimetal when spin-orbit coupling (SOC) is ignored. We also obtain the nearly flat surface state which has the drumhead characteristic. When SOC is included, three node lines evolve into a pair of Dirac points along the $M - R$ line. These Dirac points are robust and protected by C_4 rotation symmetry. Once this crystal symmetry is broken, the Dirac points will be eliminated, and the system becomes a strong topological insulator.

PACS numbers: 71.20.-b, 73.20.-r, 71.55.Ak, 73.43.-f

INTRODUCTION

Topological insulator (TI) has attracted broad interest in recent years[1, 2]. The unique property of TI is that the bulk state has a energy gap while the surface state is gapless. The topological property also have been proposed for three dimensional (3D) semimetal[3–7]. Up to now, three kinds of topological semimetal have been discovered, i.e., 3D Dirac semimetal (DSM)[7, 10–14], Weyl semimetal (WSM)[3, 4, 8, 9] and node-line semimetal (NLS)[15–18]. The 3D DSM has four-fold degeneracy point formed by two double degeneracy linear band crossing. Combining the crystal symmetry and time reversal symmetry, 3D DSM can be robust against external perturbations. Based on band structural calculation, several materials have been proposed to be 3D DSM[7, 10–14] and some of them already been confirmed by experiments[19–22]. If one breaks time reversal symmetry[3, 8, 9, 23] or inversion symmetry[24–27], the double degeneracy bands will split, consequently the 3D DSM evolves into WSM. Very recently, the predictions about WSM in TaAs family [26, 27] had been confirmed experimentally [28–31].

Unlike DSM and WSM whose band crossing points distribute at separate k points in the Brillouin zone (BZ), for the NLS, the crossing points around the Fermi level form a closed loop. Several compounds had been proposed as NLS included MTC[16], Bernal graphite[32], hyperhoneycomb lattices[33] and antiperovskite Cu_3PdN [17, 18] and Cu_3NZN [18]. When SOC is neglected, for the system with band inversion, time reversal symmetry together with inversion symmetry or mirror symmetry will guarantee node line in 3D BZ[16–18, 26, 34, 35]. Same with TI and WSM, NLS also has an characteristic surface state,

namely, *drumhead* like state[15–18]. Such 2D flat band surface state may become a route to achieve high temperature superconductivity[36, 37].

In this article, based on first-principles calculations and effective model analysis, we propose that CaTe in CsCl-type structure is a NLS with drumhead like surface flat bands when SOC is ignored. As shown in Fig. 1(b), around the M point, there are three node-line rings, which is perpendicular to each other. When SOC is included, these three node-line rings evolve into two Dirac points along the $M - R$ line. The Dirac points are robust and protected by the C_4 rotational symmetry. If the C_4 symmetry is broken, the system becomes a strong topological insulator with Z_2 indices (1;000).

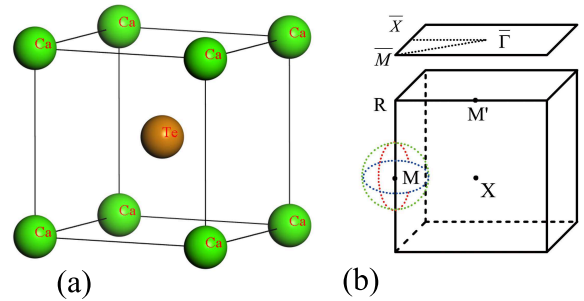


FIG. 1: (color online). (a) Crystal structure of CaTe in CsCl type phase. (b) The 3D BZ and projected (001) two dimensional (2D) BZ of CaTe. Three dash circles are the scheme of the three line nodes around the M point. The blue circle is parallel to $k_z = 0$ plane, red circle is parallel to $k_x = 0$ plane and the green circle is parallel to $k_y = 0$ plane.

CRYSTAL STRUCTURE AND METHOD

As one member of the alkaline-earth chalcogenides, CaTe have attracted tremendous interests because of its technological applications ranging from catalysis to luminescence[38–42]. CaTe undergoes a phase transition from NaCl-type structure at ambient conditions to CsCl-type structure at hydrostatic pressure about 33 GPa[38, 39]. The structure of CaTe in CsCl-type is shown in Fig.1(a). The space group of this phase is $Pm\bar{3}m$ (NO. 221). The electronic band structure calculations have been carried out using the full potential linearized augmented plane wave method as implemented in WIEN2K package [43]. To obtain accurate band inversion strength and band order, the modified Becke-Johnson exchange potential together with local-density approximation for the correlation potential (MBJLDA) has been applied [44]. The plane-wave cutoff parameter $R_{MT}K_{max}$ is set to 7 and a $16 \times 16 \times 16$ mesh was used for the BZ integral. The SOC interaction is included by using the second-order variational procedure.

ELECTRONIC STRUCTURE

Firstly, we calculate the band structure of CaTe and show the result without SOC in Fig. 2(a). By checking the wave functions, we find that the valence bands and conduction bands are mainly contributed by $5p_z$ (blue) state of Te and $3d_{z^2}$ (red) state of Ca, respectively, as shown in Fig. 2(a). The band inversion happened at M point where the energy of Te- $5p_z$ state is higher than the energy of Ca- $3d_{z^2}$ state by about 0.75 eV. Interestingly, this kind of band inversion is not caused by the SOC, which is different from most topological materials[1, 2]. We calculate the electronic structure of CaTe by applying tensile strain to check the origin of band inversion at M point. The energy difference between Te- $5p_z$ state and Ca- $3d_{z^2}$ state decreases as increasing the tensile strain. We find that when $a \geq 1.05a_0$, the band inversion at M point disappear. With the time reversal symmetry and inversion symmetry, the band inversion results in node lines as proved in Ref. [16].

The effective Hamiltonian of node line around M point can be established by using the $\vec{k} \cdot \vec{p}$ method. Considering the crystal symmetry at M point and time reversal symmetry, the effective Hamiltonian can be written as following form:

$$H(\vec{k}) = g_0(\vec{k})\sigma_0 + g_x(\vec{k})\sigma_x + g_z(\vec{k})\sigma_z,$$

where the σ_x and σ_z are Pauli matrices, σ_0 is unit matrix. $g_0(\vec{k}) = M_0 - B_0(k_x^2 + k_y^2) - C_0k_z^2$, $g_x(\vec{k}) = Ak_xk_yk_z$, $g_z(\vec{k}) = M_z - B_z(k_x^2 + k_y^2) - C_zk_z^2$. This

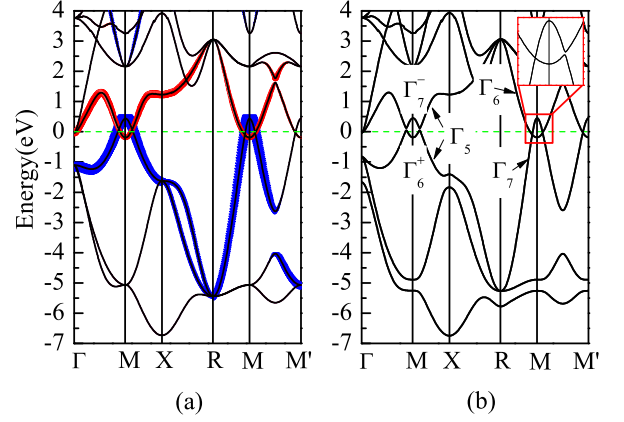


FIG. 2: (color online). (a) Electronic structure of CaTe without SOC. The weights of Te- $5p_z$ (Ca- $3d_{z^2}$) state is proportional to the width of blue (red) curves. (b) Electronic structure of CaTe with SOC. Along $\Gamma - M$, $M - X$ and $M - M'$, a small gap is opened. The Dirac point at the $M - R$ line is protected by C_4 rotational symmetry. The inset is the detailed structure around the M point. (see main text for detailed description).

system has both of time reversal symmetry and inversion symmetry, thus, the component of σ_y is zero[16]. The eigenvalues of this 2×2 effective Hamiltonian are $E(\vec{k}) = g_0(\vec{k}) \pm \sqrt{g_x^2(\vec{k}) + g_z^2(\vec{k})}$. When $g_x(\vec{k}) = 0$ and $g_z(\vec{k}) = 0$, the nodal line will emergent. It can be easily checked that the equation $g_z(\vec{k}) = 0$ has solution only when $M_zB_z > 0$ and $M_zC_z > 0$. And $M_zB_z > 0$ and $M_zC_z > 0$ are also the condition of band inversion. On the other hand, $g_x(\vec{k}) = 0$ confine the node lines in three mutually perpendicular planes (namely, $k_x=0$ plane, $k_y=0$ plane and $k_z=0$ plane) as illustrated in Fig. 1(b). Due to the fact that $g_0(\vec{k})$ does not equal to zero which breaks the electron-hole symmetry, consequently, the node lines have finite energy dispersion.

When SOC is considered, three node lines evolve into two Dirac points at $M - R$ line as shown in Fig. 2(b). At M point, the two states near Fermi level belong to irreducible representation Γ_7^- and Γ_6^+ , respectively. While along the $M - X$ line, two bands have the same irreducible representation Γ_5 as shown in Fig. 2(b), thus they can hybridize with each other and open a small gap (about 50meV). For both $\Gamma - M$ line and $M - M'$ line, the two bands around Fermi level are also belong to the same irreducible representation, thus there is not band crossing along $\Gamma - M$ line and $M - M'$ line. Since the band splitting is determined by the SOC, thus one can achieve the NLS by doping the lighter atoms such as Se, S.

Along the $M - R$ line, which reserve the C_4 rotation symmetry, two states with Γ_7^- and Γ_6^+ at M point evolve

into Γ_7 and Γ_6 , thus the hybridization between these two bands is forbidden, there is a Dirac point as shown in Fig.2(b). When the C_4 rotational symmetry is broken, like by strain effect, the band crossing point will disappear, and this 3D DSM will become a strong TI with topological indices Z_2 to be (1;0,0,0).

To understand the band inversion at M point and the topological property of this system, we derive a low energy effective Hamiltonian at M point based on the

$$H_{eff} = \begin{pmatrix} M_1(\vec{k}) & 0 & Ak_+ + B(\vec{k}) & D(\vec{k}) \\ 0 & M_1(\vec{k}) & D^*(\vec{k}) & -Ak_- - B^*(\vec{k}) \\ Ak_- + B^*(\vec{k}) & D(\vec{k}) & M_2(\vec{k}) & 0 \\ D^*(\vec{k}) & -Ak_+ - B(\vec{k}) & 0 & M_2(\vec{k}), \end{pmatrix}$$

where $M_1(\vec{k}) = M_{10} + M_{11}(k_x^2 + k_y^2) + M_{12}k_z^2$, $M_2(\vec{k}) = M_{20} + M_{21}(k_x^2 + k_y^2) + M_{22}k_z^2$, $B(\vec{k}) = B_1k_+k_z^2 + B_2(k_x^3 + ik_y^3) + iB_3k_-k_xk_y$, $D(\vec{k}) = D_1(k_x^2 - k_y^2)k_z + iD_2k_xk_yk_z$, $k_{\pm} = k_x \pm ik_y$. Along the k_z axis (where $k_x=0, k_y=0$) the effective Hamiltonian is diagonal, and the eigenvalues are $E(\vec{k}) = M_1(\vec{k})$ and $E(\vec{k}) = M_2(\vec{k})$. As mentioned above, the Dirac point is on the $M-R$ line, thus it is interesting to discuss the effective model along this line. Since there is the band inversion between $|j_z = \pm\frac{1}{2}\rangle_d$ and $|j_z = \pm\frac{3}{2}\rangle_p$ at M point, it is easy to obtain that $M_{10} < M_{20}$, $M_{22} < 0 < M_{12}$, and the Dirac points locate at $\vec{k}_c = (\frac{\pi}{a}, \frac{\pi}{a}, k_{zc} = \pm\sqrt{\frac{M_{20}-M_{10}}{M_{12}-M_{22}}})$. Neglecting the high-order terms, $E(\vec{k}_c + \delta\vec{k})$ can be expressed as $(M_{12} + M_{22})k_{zc}\delta k_z \pm \sqrt{(M_{12} - M_{22})^2k_{zc}^2\delta k_z^2 + A^2(\delta k_x^2 + \delta k_y^2)}$, where $\delta k_{x,y,z}$ are small displacement from \vec{k}_c . In the vicinity of \vec{k}_c , the band dispersion is a linear, thus our effective Hamiltonian is nothing but 3D massless Dirac fermions.

The band inversion at M point and the Dirac nodes in CaTe suggest the existence of topological nontrivial surface state. To study the surface states in CaTe we use a 200-unit-cells-thick (001) slab with top (bottom) surface terminated by Ca (Te) atoms. The surface state is then calculated by using the tight-binding method. The hopping parameters are determined from a maximally localized Wannier functions (MLWFs)[45], which are projected from the Bloch state derived from first-principles calculations.

Fig. 3(a)/(b) shows the surface state of CaTe (001) surface without/with SOC, respectively. When SOC is ignored, the system is a NLS, and possess nearly flat sur-

face band around the Fermi energy. As shown in Fig. 3(a), our numerical results find that the nearly flat surface "drumhead" state appears in the interiors of the projected nodal line rings on the (001) surface around the \bar{M} point. Since the slab we used has two surfaces, there are

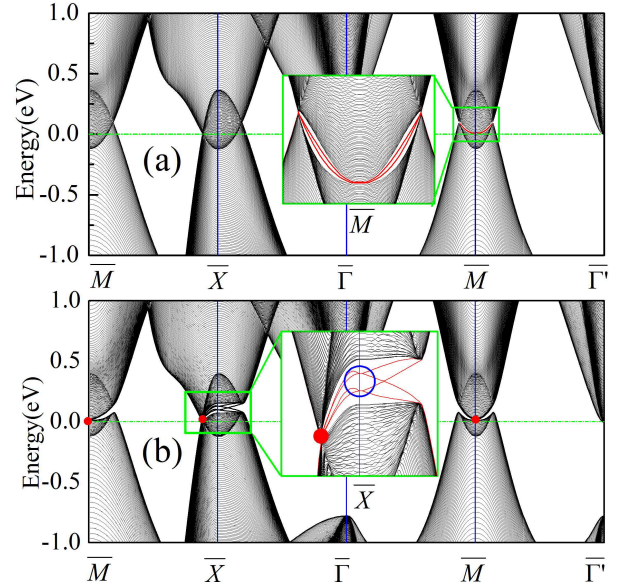


FIG. 3: (color online). The surface state of (001) surface of CaTe. (a) The surface state is calculated without SOC. The flat surface state around Fermi level is denoted by red color. The inset is the detailed band structure around the \bar{M} point. (b) The surface state is calculated with SOC. The red dots are the projected bulk Dirac nodes. The red lines between the bulk gap at \bar{X} point are surface states and the blue circle denotes the surface Dirac cones. The inset is the detailed band structure around the \bar{X} point.

face band around the Fermi energy. As shown in Fig. 3(a), our numerical results find that the nearly flat surface "drumhead" state appears in the interiors of the projected nodal line rings on the (001) surface around the \bar{M} point. Since the slab we used has two surfaces, there are

two surface states as shown in the red lines in the Fig. 3(a). The particle-hole symmetry is broken by nonzero term $g_0(\vec{k})$, thus these two surface bands are not perfect flat with about 70 meV bandwidth. This type of 2D flat bands are proposed as a novel route to achieve high temperature superconductivity[36, 37].

When the SOC is included, three node lines are gapped out and become a pair of Dirac points along the $M - R$ line, thus the NLS become a 3D DSM. There is bulk Dirac node projected on \overline{M} point (the red dot) as shown in Fig. 3(b). Along the $\overline{M} - \overline{X}$, there is also a projected bulk Dirac node, which locate near the \overline{X} point denoted by red dots. Fig. 3(b) is clearly shows that the gapped bulk states along the $\overline{\Gamma} - \overline{X}$ direction and the existence of surface Dirac cones (in the blue circle) due to the topologically nontrivial Z_2 indices, like the same case in Na_3Bi [11] and Cd_3As_2 [12].

CONCLUSION

In summary, based on first-principles calculations and effective model analysis, we suggest that CaTe in CsCl-type structure is a NLS when SOC is ignored. There are three node-line rings which are perpendicular to each other around the M point. With band inversion at M point, this NLS is protected by the time reversal symmetry and inversion symmetry. When the SOC is included, three node-line rings become a pair of Dirac points. These Dirac nodes are robust and protected by the C_4 crystal symmetry and the system become a DSM.

ACKNOWLEDGEMENT

The work was supported by the National Key Project for Basic Research of China (Grant No. 2014CB921104), NSFC under Grants No. 11525417 and 11374147. The project is also funded by Priority Academic Program Development of Jiangsu Higher Education Institutions. S.S. were supported by NSF DMR (Grant No. 1411336). Y.D. is supported by the program B for Outstanding PhD candidate of Nanjing University.

APPENDIX

The conduction and valence bands of CaTe at M point are mainly contributed by four states: $|j_z = -\frac{1}{2}\rangle_d$, $|j_z = +\frac{1}{2}\rangle_d$, $|j_z = -\frac{3}{2}\rangle_p$ and $|j_z = +\frac{3}{2}\rangle_p$, we thus use these states as the basis to build the effective model Hamiltonian at the M point of BZ. As a 4×4 Hermitian matrix, the effective Hamiltonian can be expended as $H = \sum_{i=1}^{16} f_i(\vec{k}) \Gamma_i$, where $f_i(\vec{k})$ are function of momentum \vec{k} . Γ_i are Dirac matrices, which can be written as

the direct product of σ_i and τ_j ($\sigma_{i=1,2,3,4}$, $\tau_{j=1,2,3,4}$ are unit matrix σ_0 and three Pauli matrices σ_x , σ_y and σ_z).

Under the operation of crystal symmetry and time reversal symmetry, the Hamiltonian should be invariant. This requires the function $f_i(\vec{k})$ and the associated Γ_i matrices belong to the same irreducible representation. Thus the key problem is to determine the irreducible representation for $f_i(\vec{k})$ and Γ_i matrices, which can be done by the projection-operator method.

Because the SOC is included, we use the double space group. Under the projection-operator method, we present the irreducible representation of Dirac Γ matrices and polynomials of \vec{k} , and their transformation under time reversal in Table I. With the Table I, the effective model Hamiltonian of CaTe at M point can be easily expressed as: $H = f_1(\vec{k})\Gamma_1 + f_{13}(\vec{k})\Gamma_{13} + f_8(\vec{k})\Gamma_8 - f_9(\vec{k})\Gamma_9 + D_1(k_x^2 - k_y^2)k_z\Gamma_6 - D_2k_xk_yk_z\Gamma_7$, where $f_1(\vec{k}) = C_1 + m_1(k_x^2 + k_y^2) + n_1k_z^2$, $f_{13}(\vec{k}) = C_{13} + m_{13}(k_x^2 + k_y^2) + n_{13}k_z^2$, $f_8(\vec{k}) = Ak_x + B_1k_x^3 + B_2k_xk_z^2 + B_3k_y^2k_x$, $f_9(\vec{k}) = Ak_y + B_1k_y^3 + B_2k_yk_z^2 + B_3k_x^2k_y$. $\Gamma_1 = \sigma_0 \otimes \tau_0$, $\Gamma_{13} = \sigma_3 \otimes \tau_0$, $\Gamma_8 = \sigma_1 \otimes \tau_3$, $\Gamma_9 = \sigma_2 \otimes \tau_0$, $\Gamma_6 = \sigma_1 \otimes \tau_1$, $\Gamma_7 = \sigma_1 \otimes \tau_2$. Compare with the effective Hamiltonian, we have $M_{10}(M_{20}) = C_1 \pm C_{13}$, $M_{11}(M_{21}) = m_1 \pm m_{13}$, $M_{12}(M_{22}) = n_1 \pm n_{13}$.

* Corresponding author: xgwan@nju.edu.cn

- [1] M. Z. Hasan and C. L. Kane, Rev. Mod. Phys. **82**, 3045 (2010).
- [2] X. L. Qi and S.-C. Zhang, Rev. Mod. Phys. **83**, 1057 (2011).
- [3] X. Wan, A. M. Turner, A. Vishwanath, and S. Y. Savrasov, Phys. Rev. B **83**, 205101 (2011).
- [4] L. Balents, Physics **4**, 36 (2011).
- [5] Y. Ando, J. Phys. Soc. of Jpn. **82**, 102001 (2013).
- [6] K.-Y. Yang, Y.-M. Lu, and Y. Ran, Phys. Rev. B **84**, 075129 (2011).
- [7] T. O. Wehling, A. M. Black-Schaffer, and A. V. Balatsky, Adv. Phys. **63**, 1 (2014).
- [8] G. Xu, H. M. Weng, Z. Wang, X. Dai, and Z. Fang, Phys. Rev. Lett. **107**, 186806 (2011).
- [9] A. A. Burkov and Leon Balents, Phys. Rev. Lett. **107**, 127205 (2011).
- [10] S. M. Young, S. Zaheer, J. C. Y. Teo, C. L. Kane, E. J. Mele, and A. M. Rappe, Phys. Rev. Lett. **108**, 140405 (2012).
- [11] Z. Wang, Y. Sun, X.-Q. Chen, C. Franchini, G. Xu, H. M. Weng, X. Dai, and Z. Fang, Phys. Rev. B **85**, 195320 (2012).
- [12] Z. Wang, H. M. Weng, Q. Wu, X. Dai, and Z. Fang, Phys. Rev. B **88**, 125427 (2013).
- [13] Y. Du, B. Wan, D. Wang, L. Sheng, C. Duan and X. Wan, Sci. Rep. **5**, 14423 (2015).
- [14] Q. D. Gibson, L. M. Schoop, L. Muechler, L. S. Xie, M. Hirschberger, N. P. Ong, R. Car, and R. J. Cava Phys.

Γ matrices	representation	T
Γ_1, Γ_{13}	R_1	+
Γ_4, Γ_{16}	R_2	-
$\{\Gamma_2, \Gamma_3\}, \{\Gamma_{14}, \Gamma_{15}\}$	R_5	-
Γ_7	R_{10}	-
Γ_{11}	R_{10}	+
Γ_6	R_{11}	-
Γ_{10}	R_{11}	+
$\{\Gamma_8, \Gamma_9\}$	R_{12}	-
$\{\Gamma_5, \Gamma_{12}\}$	R_{12}	+
$d(k)$	representation	T
$C, k_z^2, k_x^2 + k_y^2$	R_1	+
$k_x^2 - k_y^2$	R_3	+
$k_x k_y$	R_4	+
$\{k_x k_z, k_y k_z\}$	R_5	+
$k_z, k_z^3, (k_x^2 + k_y^2)k_z$	R_9	-
$k_x k_y k_z$	R_{10}	-
$\{k_x^2 - k_y^2\}k_z$	R_{11}	-
$(k_x, k_y), (k_x^3, k_y^3), (k_x^2 k_y, k_y^2 k_x), (k_x k_z^2, k_y k_z^2)$	R_{12}	-

TABLE I: The character table of Dirac Γ matrices and the polynomials of the momentum k for CaTe at M point.

- Rev. B **91**, 205128 (2015).
- [15] A. A. Burkov, M.D. Hook, and L. Balents, Phys. Rev. B **84**, 235126 (2011)
- [16] H. Weng, Y. Liang, Q. Xu, R. Yu, Z. Fang, X. Dai, and Y. Kawazoe, Phys. Rev. B **92**, 045108 (2015)
- [17] R. Yu, H. Weng, Z. Fang, X. Dai and X. Hu, Phys. Rev. Lett. **115**, 036807 (2015)
- [18] Y. Kim, B. J. Wieder, C. L. Kane, and A. M. Rappe, Phys. Rev. Lett. **115**, 036806 (2015)
- [19] S. Jeon, B. B. Zhou, A. Gyenis, B. E. Feldman, I. Kimchi, A. C. Potter, Q. D. Gibson, R. J. Cava, A. Vishwanath, and A. Yazdani, Nat. Mater. **13**, 851 (2014).
- [20] M. Neupane, S.-Y. Xu, R. Sankar, N. Alidoust, G. Bian, C. Liu, I. Belopolski, T.-R. Chang, H.-T. Jeng, H. Lin, A. Bansil, F. Chou, and M. Z. Hasan, Nat. commun. **5**, 3786 (2014).
- [21] Z. K. Liu, B. Zhou, Y. Zhang, Z. J. Wang, H. M. Weng, D. Prabhakaran, S.-K. Mo, Z. X. Shen, Z. Fang, X. Dai, Z. Hussain, and Y. L. Chen, Science **343**, 864 (2014).
- [22] Z. K. Liu, J. Jiang, B. Zhou, Z. J. Wang, Y. Zhang, H. M. Weng, D. Prabhakaran, S. K. Mo, H. Peng, P. Dudin, T. Kim, M. Hoesch, Z. Fang, X. Dai, Z. X. Shen, D. L. Feng, Z. Hussain, and Y. L. Chen, Nature Materials **13**, 677 (2014).
- [23] X. Wan, A. Vishwanath, and S. Y. Savrasov, Phys. Rev. Lett. **108**, 146601 (2012).
- [24] G. B. Halasz and L. Balents, Phys. Rev. B **85**, 035103 (2012).
- [25] J. Liu and D. Vanderbilt, Phys. Rev. B **90**, 155316 (2014).
- [26] H. Weng, C. Fang, Z. Fang, B. A. Bernevig, and X. Dai, Phys. Rev. X **5**, 011029 (2015).
- [27] S. M. Huang, S. Y. Xu, I. Belopolski, C. C. Lee, G. Chang, B. Wang, N. Alidoust, G. Bian, M. Neupane, C. Zhang, S. Jia, A. Bansil, H. Lin, and M. Z. Hasan, Nat. commun. **6**, 7373 (2015).
- [28] B. Q. Lv, H. M. Weng, B. B. Fu, X. P. Wang, H. Miao, J. Ma, P. Richard, X. C. Huang, L. X. Zhao, G. F. Chen, Z. Fang, X. Dai, T. Qian, and H. Ding, Phys. Rev. X **5**, 031013 (2015).
- [29] B. Q. Lv, N. Xu, H. M. Weng, J. Z. Ma, P. Richard, X. C. Huang, L. X. Zhao, G. F. Chen, C. E. Matt, F. Bisti, V. N. Strocov, J. Mesot, Z. Fang, X. Dai, T. Qian, M. Shi and H. Ding, Nat. Phys. **11**, 724–727 (2015).
- [30] S.-Y. Xu, I. Belopolski, N. Alidoust, M. Neupane, G. Bian, C. Zhang, R. Sankar, G. Chang, Z. Yuan, C.-C. Lee, S.-M. Huang, H. Zheng, J. Ma, D. S. Sanchez, B. Wang, A. Bansil, F. Chou, P. P. Shibayev, H. Lin, S. Jia, M. Z. Hasan, Science **349**, 613 (2015).
- [31] S.-Y. Xu, N. Alidoust, I. Belopolski, Z. Yuan, G. Bian, T.-R. Chang, H. Zheng, V. N. Strocov, D. S. Sanchez, G. Chang, C. Zhang, D. Mou, Y. Wu, L. Huang, C.-C. Lee, S.-M. Huang, B. Wang, A. Bansil, H.-T. Jeng, T. Neupert, A. Kaminski, H. Lin, S. Jia and M. Z. Hasan, Nat. Phys. **11**, 748–754 (2015).
- [32] T. T. Heikkila and G. E. Volovik, arXiv: 1504.05824v1 (2015.)
- [33] K. Mullen, B. Uchoa, and D. T. Glatzhofer, Phys. Rev. Lett. **115**, 026403 (2015).
- [34] L. S. Xie, L. M. Schoop, E. M. Seibel, Q. D. Gibson, W. Xie, and R. J. Cava, APL Materials **3**, 083602 (2015).
- [35] M. Zeng, C. Fang, G. Chang, Y. A. Chen, T. Hsieh, A. Bansil, H. Lin, L. Fu, arXiv:1504.03492 (2015)
- [36] T. T. Heikkila and G. E. Volovik, arXiv: 1504.05824 (2015)
- [37] N. B. Kopnin, T. T. Heikkila, and G. E. Volovik, Phys. Rev. B **83**, 220503 (2011).
- [38] H. G. Zimmer, H. Winzen, and K. Syassen, Phys. Rev. B **32**, 4066 (1985).
- [39] H. Luo, R. G. Greene, K. Ghandehari, T. Li, and A. L. Ruoff, Phys. Rev. B **50**, 16232 (1994).
- [40] M. Dadsetani and A. Pourghazi, Phys. Rev. B **73**, 195102

- (2006).
- [41] S. Boucenna, Y. Medkour, L. Louail, M. Boucenna, A. Hachemi, A. Roumili, *Comput. Mater. Sci.* **68**, 325 (2013).
 - [42] D. Varshneya, V. Rathore, R. Kinger, R. K. Singh, *J. Alloys Compd.* **484**, 239 (2009).
 - [43] P. Blaha, K. Schwarz, G. K. H. Madsen, D. Kvasnicka, and J. Luitz, WIEN2K, An Augmented Plane Wave+ Local Orbitals Program for Calculating Crystal Properties (Karlheinz Schwarz, Technische Universitat Wien, Austria, 2001).
 - [44] F. Tran and P. Blaha, *Phys. Rev. Lett.* **102**, 226401 (2009).
 - [45] N. Marzari, A. A. Mostofi, J. R. Yates, I. Souza, and D. Vanderbilt, *Rev. Mod. Phys.* **84**, 1419 (2012)